REPORT DOCUMENTATION PAGE

Form Approved OMB NO. 0704-0188

The public reporting burden for this collection of information is estimated to average 1 hour per response, including the time for reviewing instructions, searching existing data sources, gathering and maintaining the data needed, and completing and reviewing the collection of information. Send comments regarding this burden estimate or any other aspect of this collection of information, including suggesstions for reducing this burden, to Washington Headquarters Services, Directorate for Information Operations and Reports, 1215 Jefferson Davis Highway, Suite 1204, Arlington VA, 22202-4302. Respondents should be aware that notwithstanding any other provision of law, no person shall be subject to any oenalty for failing to comply with a collection of information if it does not display a currently valid OMB control number.
PLEASE DO NOT RETURN YOUR FORM TO THE ABOVE ADDRESS.

1. REPORT DATE (DD-MM-YYYY)	2. REPORT TYPE	3. DATES COVERED (From - To)
21-09-2015	Manuscript	-

4. TITLE AND SUBTITLE
Water Activated Doping and Transport in Multilayered Germanane Crystals

5a. CONTRACT NUMBER
W911NF-12-1-0481

5b. GRANT NUMBER

5c. PROGRAM ELEMENT NUMBER
611102

6. AUTHORS
Justin Young, Basant Chitara , Nicholas Cultrara , Maxx Q Arguilla , Shishi Jiang, Fan Fan , Ezekiel Johnston-Halperin, Joshua E Goldberger

5d. PROJECT NUMBER

5e. TASK NUMBER

5f. WORK UNIT NUMBER

7. PERFORMING ORGANIZATION NAMES AND ADDRESSES
Ohio State University
1960 Kenny Road

Columbus, OH 43210 -1016

8. PERFORMING ORGANIZATION REPORT NUMBER

9. SPONSORING/MONITORING AGENCY NAME(S) AND ADDRESS (ES)
U.S. Army Research Office
P.O. Box 12211
Research Triangle Park, NC 27709-2211

10. SPONSOR/MONITOR'S ACRONYM(S)
ARO

11. SPONSOR/MONITOR'S REPORT NUMBER(S)
62249-MS.11

12. DISTRIBUTION AVAILIBILITY STATEMENT
Approved for public release; distribution is unlimited.

13. SUPPLEMENTARY NOTES
The views, opinions and/or findings contained in this report are those of the author(s) and should not contrued as an official Department of the Army position, policy or decision, unless so designated by other documentation.

14. ABSTRACT
The synthesis of germanane (GeH) has opened the door for covalently-functionalizable two-dimensional materials in electronics. Herein, we demonstrate that GeH can be electronically doped by incorporating stoichiometric equivalents of phosphorus dopant atoms into the CaGe2 precursor. The electronic properties of these doped materials show significant atmospheric sensitivity, and we observe a reduction in resistance by up to three orders of magnitude when doped samples are measured in water-containing atmospheres. This variation in resistance is a result of water activation of the phosphorus dopants. Transport measurements in different contact geometries show

15. SUBJECT TERMS
2D Materials, Germanane, Electronic Transport

16. SECURITY CLASSIFICATION OF:			17. LIMITATION OF ABSTRACT	15. NUMBER OF PAGES	19a. NAME OF RESPONSIBLE PERSON
a. REPORT	b. ABSTRACT	c. THIS PAGE			Joshua Goldberger
UU	UU	UU	UU		19b. TELEPHONE NUMBER 614-247-7438

Standard Form 298 (Rev 8/98)
Prescribed by ANSI Std. Z39.18

Report Title

Water Activated Doping and Transport in Multilayered Germanane Crystals

ABSTRACT

The synthesis of germanane (GeH) has opened the door for covalently-functionalizable two-dimensional materials in electronics. Herein, we demonstrate that GeH can be electronically doped by incorporating stoichiometric equivalents of phosphorus dopant atoms into the CaGe2 precursor. The electronic properties of these doped materials show significant atmospheric sensitivity, and we observe a reduction in resistance by up to three orders of magnitude when doped samples are measured in water-containing atmospheres. This variation in resistance is a result of water activation of the phosphorus dopants. Transport measurements in different contact geometries show a significant anisotropy between in-plane and out-of-plane resistances, with a much larger out-of-plane resistance. These measurements along with finite element modeling results predict that the current distribution in top contacted crystals is restricted to only the topmost, water activated crystal layers. Taken together, these results pave the way for future electronic and optoelectronic applications utilizing group IV graphane analogues.

Water Activated Doping and Transport in Multilayered Germanane Crystals

Justin R Young[1], Basant Chitara[2], Nicholas D Cultrara[2], Maxx Q Arguilla[2], Shishi Jiang[2], Fan Fan[2] Ezekiel Johnston-Halperin[1], Joshua E Goldberger[2]

[1] Department of Physics, The Ohio State University, Columbus, OH 43210.

[2] Department of Chemistry and Biochemistry, The Ohio State University, Columbus, OH 43210.

Email: goldberger@chemistry.ohio-state.edu

Abstract. The synthesis of germanane (GeH) has opened the door for covalently-functionalizable two-dimensional materials in electronics. Herein, we demonstrate that GeH can be electronically doped by incorporating stoichiometric equivalents of phosphorus dopant atoms into the $CaGe_2$ precursor. The electronic properties of these doped materials show significant atmospheric sensitivity, and we observe a reduction in resistance by up to three orders of magnitude when doped samples are measured in water-containing atmospheres. This variation in resistance is a result of water activation of the phosphorus dopants. Transport measurements in different contact geometries show a significant anisotropy between in-plane and out-of-plane resistances, with a much larger out-of-plane resistance. These measurements along with finite element modeling results predict that the current distribution in top contacted crystals is restricted to only the topmost, water activated crystal layers. Taken together, these results pave the way for future electronic and optoelectronic applications utilizing group IV graphane analogues.

Keywords. germanane, graphane analogues, electronic transport, 2D materials

1. Introduction

Over the past decade, there has been considerable scientific interest focused around the unique properties and device applications of single sheet and multilayered van der Waals materials [1-6]. When exfoliated or grown as single atomic layers, many of these two-dimensional (2D) materials exhibit electronic and optoelectronic properties which differ fundamentally from those of the parent bulk materials [7, 8]. These changes are indicative of the small but appreciable electronic coupling that arises between the neighboring layers of these bulk crystals. For instance, single-layered graphene exhibits the quantum Hall effect at room temperature. This is not seen in its bulk counterpart, graphite, and demonstrates graphene's high-mobility two-dimensional electronic structure [9]. Additionally, the normally indirect band gaps of the group VIB layered transition metal dichalcogenides, such as MoS_2, transform into direct band gaps only when exfoliated or grown as single layers [10-13]. This dramatic contrast between single- and multi-layered 2D crystals implies that there exists significant coupling between the different layers. In contrast, a material where this interlayer coupling is strongly suppressed or can be manipulated would enable observation of these exotic 2D phenomena even in relatively thick multilayered crystals.

The Si/Ge/Sn graphane analogues are a unique class of van der Waals materials that feature a 2D electronically active main group lattice in which every atom is terminated with a covalent ligand [14-17]. This covalent termination serves to dramatically suppress band dispersion in the out-of-plane direction as compared to previously studied van der Waals materials. Furthermore, varying the identity of the covalently terminated ligand enables tuning of the in-plane and out-of-plane electronic and thermal transport behavior, optical properties, thermal stability, and topological phases in these materials [16, 18-20]. The recent development of a facile approach to the synthesis of Ge graphane analogues has resulted in mm-scale crystals of both hydrogen-terminated germanane (GeH) and methyl-terminated germanane ($GeCH_3$) [14, 16, 21]. Hydrogen-terminated germanane is of particular interest due to the predictions of a room temperature phonon-limited electron mobility of 18,000 $cm^2/V{\cdot}s$—a value approximately five times larger than the mobility in bulk Ge—and a direct bandgap of 1.59 eV. Density functional theory predicts little change in the electronic structure between an isolated sheet of GeH, and the two-layer unit cell [16]. Consequently, there is only a weak electronic coupling between crystal layers. Therefore, the high mobility and direct band gap are predicted to exist both in exfoliated flakes and in the bulk crystalline material. While studies on electronic transport in silicene and related silicon based graphane analogues exist, to date there have been none on the germanium based graphane analogues [22, 23].

Herein, we measure for the first time the electrical transport properties of GeH through measurements on both undoped and phosphorous doped GeH multilayer crystals. Dopants are incorporated into the GeH lattice by first integrating stoichiometric equivalents of the elemental dopants into the precursor $CaGe_2$ Zintl

phase. The effectiveness of this phosphorous doping is verified by observation of a reduction in sheet resistance by up to three orders of magnitude. There is also a significant anisotropy between electronic transport parallel and perpendicular to the layered structure. Additionally, there is a strong atmospheric dependence in the resistance, with the sample resistance decreasing when water vapor is present in the environment. These results, combined with a finite element analysis of the transport in GeH, are used to extract the in-plane and out-of-plane resistivities and to model the current distribution in GeH crystals. This suggest that the sample current flows primarily through the outermost layers due to dopant activation by the water vapor present in the environment. This dopant activation results in a modeled resistivity four orders of magnitude smaller than those calculated in vacuum.

2. Experimental Methods

Single-crystalline flakes of GeH were synthesized using methods previously reported [8]. In brief, the layered $CaGe_2$ Zintl phase precursor was produced by annealing a stoichiometric ratio of calcium and germanium in a sealed quartz tube at 950-1050 °C under vacuum. The samples were subsequently cooled over the course of 2-10 days. The $CaGe_2$ crystals were then converted to GeH by treatment in concentrated HCl for 5-14 days at -40 °C. This process yielded GeH crystals which measure up to 4 mm laterally and have a thickness of 5-20 μm. To tune the electronic properties of the resulting GeH, phosphorous was used as an extrinsic n-type dopant. Phosphorous doped GeH crystals (P:GeH) were obtained by incorporating stoichiometric amounts of phosphorous—0.5 and 1.0% atomic percentage—to the initial Ca/Ge mixture, followed by the same annealing and HCl treatment processes used for the undoped GeH synthesis.

The crystallinity of the resulting GeH and P:GeH crystals was confirmed via powdered x-ray diffraction (XRD), Raman spectroscopy, and scanning electron microscopy (SEM). XRD was performed on a Bruker D8 powder X-ray diffractometer with Cu Kα radiation. The Raman scattering spectra were collected on Renishaw InVia Raman equipped with a CCD detector using a 633 nm He-Ne laser for excitation. The SEM micrographs were taken using a FEI Helios Nanolab 600 dual beam focused ion beam and scanning electron microscope at current of 43 pA and voltage of 10 kV.

Top-contacted GeH samples were fabricated by electron-beam deposition of Ag/Au (100/20 nm) through a shadow mask, creating a 25 μm channel between the two contacts. Depositions were conducted with the sample at room temperature to avoid amorphization which occurs above 75 °C [16]. Silver (with a Au capping layer to prevent oxidation) was selected as a contact metal after showing that the silver contacts on P:GeH had smaller resistances and linear I-V curves indicating a low contact resistance and minimal Schottky barrier. Other metals tested were Ti/Au, Au, Pd, Cr, and Pt. Connections to the electron beam deposited sample contacts were made by connecting thin Au wires to the deposited contacts using Ag

epoxy. The out-of-plane samples were fabricated by placing a drop of Ag epoxy on a SiO_2/Si substrate (300nm SiO_2), setting the GeH flake on top of this epoxy, and then placing a second epoxy spot on the top of the flake. Here again, Au wire was used to make contact to the epoxy contacts.

Transport current-voltage scans were measured using a Keithley 4200-SCS, using a probe station manufactured by Lake Shore Cryotronics Inc. (Westerville, OH). Unless otherwise noted, all I-V curves are measured in ambient atmosphere, at room temperature, and in a dark environment (to prevent photo-excited carrier contributions to the conductivity).

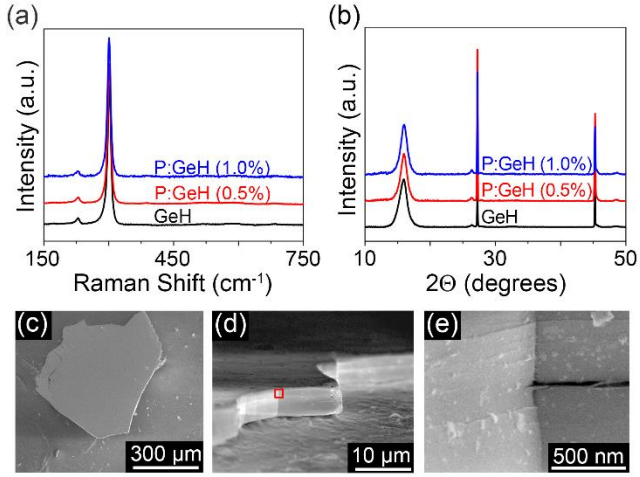

Figure 1. Raman (a) and XRD (b) spectra of HCl deintercalated GeH with 0.0% (undoped, black), 0.5% (red), and 1.0% (blue) phosphorous incorporation in the $CaGe_2$ precursor. (c-e) SEM images of the bulk GeH crystals.

3. Results and Discussion

3.1 Sample Characterization

The purity of the resulting P:GeH crystals is confirmed through X-ray crystal diffraction (XRD) and Raman spectroscopy (figure 1(a) and (b)). The samples can be indexed to a hexagonal unit cell with a = 3.880 Å and c = 11.04 Å (two GeH layers per c-unit cell spacing), consistent with previous measurements [16, 21]. The XRD spectra indicate that there are no additional impurity phases or significant changes in the lattice parameters for the doped samples. The Raman spectra of the GeH and P:GeH samples show the expected E_2 mode at 302 cm^{-1} as well as the A_1 mode at 228 cm^{-1} with no discernable changes in peak-shape or position [16, 21]. Scanning electron micrographs (figure 1(c), (d), and (e)) of the GeH crystals confirm that they are smoothly faceted with no visible gaps between the GeH sheets.

3.2 Atmospheric Dependence and Anisotropy of Resistance Measurements

In bulk crystalline samples of 2D materials, there is typically a strong anisotropy (ranging from 2-6 orders of magnitude) between resistivity in the plane of the 2D sheets and between the sheets [23-26]. In order to probe this anisotropy, as well as the effectiveness of the P dopants, two different contact geometries were employed to measure current-voltage (I-V) scans. The in-plane (IP) conductivity was probed through the use of a top contact (TC) geometry (figure 2(a), 2(b) inset), while an out-of-plane (OOP) geometry (figure 2(c), 2(d) inset) was used to measure the interplane resistivity.

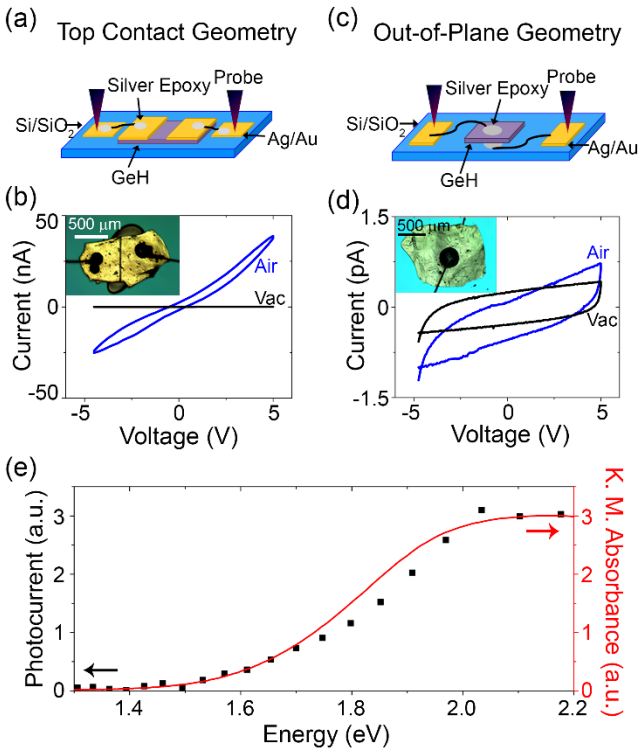

Figure 2. Schematics of the top-contact (a) and out-of-plane (c) geometries used to study the transport properties in GeH crystals. (b) and (d) show representative IV curves both in ambient atmospheric conditions (blue) and in a vacuum of 5×10^{-4} mbar (black). Out-of-plane measurements are at the lower limit of the hardware setup. Insets show characteristic micrographs of samples (e) Photocurrent as a function of light energy which matches the absorbance curve from Bianco *et al.* showing an increase in conductivity with exposure to above bandgap light [16].

Representative I-V curves for TC and OOP geometries are shown in figures 2(b) and (d), respectively (data shown here for 0.5% P:GeH). In addition to the large difference in resistances between the two contact geometries (extracted from the slopes of the IV curves), there is also a variation in the sensitivity of the two measurements to the environmental conditions. In particular, measurements conducted on TC devices show an increase in current by three orders of magnitude when exposed to the ambient atmosphere compared to measurements under a vacuum of 5×10^{-4} mbar. In contrast, the OOP devices experience almost no change in resistivity as both vacuum and ambient atmosphere measurements exhibit currents at the lower limit of the hardware setup. This lack of variation could be due to an absence of atmospheric sensitivity in the OOP conduction, or the magnitude of this change is beyond our current sensitivity. To confirm that the observed TC geometry's low current signals are generated by transport through the P:GeH crystal rather than through parallel conduction channels such as the substrate or a surface water layer, variable wavelength photoconductivity measurements were performed at light energies of 1.2-2.2 eV under vacuum. Figure 2(e) shows the photocurrent signal (black data) on top of the diffuse reflectance absorption measured previously by Bianco *et al.* in GeH (red data) [16]. The increase in photocurrent at wavelengths above the 1.59 eV bandgap correlates well with the absorption spectra and confirms that the current measured is due to conduction inside the P:GeH samples.

Since the photoconductivity measurement confirms that the conduction is occurring in the GeH crystal, the atmospheric dependence observed in the TC geometry suggests that a component of the ambient atmosphere may be activating dopants on the surface of the P:GeH crystals. Figure 3 shows the positive voltage I-V scans for a prototypical 0.5% P:GeH sample in the TC geometry upon exposure to a variety of

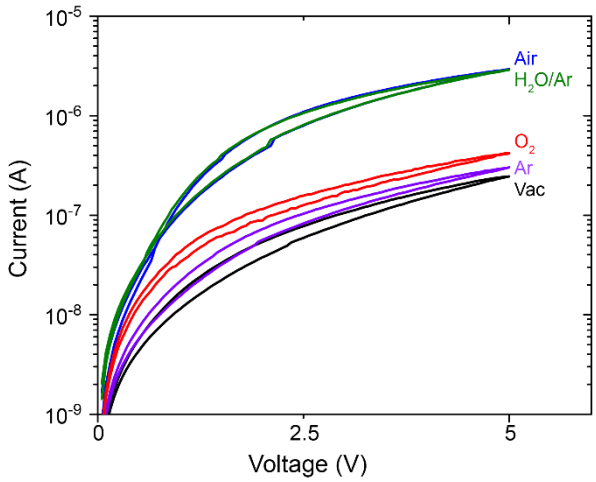

Figure 3. Representative positive voltage I-V curves showing the atmosphericic dependence of P:GeH using top contact geometry. Samples was exposed to air (blue), water/argon mixture (green), oxygen (red), argon (violet), and vacuum (black). The sample was pumped down to a base vacuum of 5×10^{-4} mbar between measurements.

atmospheres. Negative scans show similar behavior and can be found in the supplemental material (figure S1). The sample was first measured in air and then the chamber was pumped down to a vacuum of 5×10^{-4} mbar for a second measurement. The chamber was subsequently backfilled to atmospheric pressure with Ar, O_2, and 32 mbar water in argon mixture (H_2O/Ar). The system was pumped down to the base pressure after each gas exposure. On exposure to both air and water vapor, the maximum current increased as compared to the vacuum, Ar, and O_2 I-V scans. These measurements demonstrate that the component of the ambient atmosphere responsible for the decreased resistivity signal in the TC measurements is the water vapor.

3.3 Doping Dependence

Next the changes in electronic properties in samples with different phosphorous incorporation were probed in both the TC and OOP geometries. We investigate three cases: undoped GeH, 0.5% P incorporation, and 1.0% P incorporation. Figure 4 shows the respective I-V curves at different phosphorous incorporations for the TC geometry (figure 4(a)) and the OOP geometry (figure 4(b)). The TC devices show an increase in resistance by three orders of magnitude under increased phosphorous doping, while the OOP geometry show no apparent increase. Here again, all of the OOP measurements show currents that are at the hardware limits. The variation in sheet resistance of the different phosphorous incorporation regimes is shown quantitatively in figure 4(c) for the TC measurement geometry. Resistances were extracted from the slope of the best fit line for each I-V with three to five samples measured at each P incorporation value. In order to account for sample-to-sample geometric effects in the extracted resistances, the resistances were converted to sheet resistances. Error bars represent the sample to sample variation observed in the doping series measurements.

While the large resistance anisotropy of the TC and OOP contact geometries is a useful metric, the intrinsic in-plane and out-of-plane resistivities (ρ_x and ρ_z, respectively) and the anisotropy ($A = \rho_z/\rho_x$) between them provide insight into the inter- and intra-layer coupling of the material. The OOP resistivity

(ρ_z) can be extracted directly from the OOP measurement geometry using the standard equation for uniformly distributed current flow inside a material:

$$\rho_z = R_{OOP}\left(\frac{WL}{T}\right)$$

Where R_{OOP} is the resistance measured in the OOP geometry, W and L are the two in-plane sample dimensions, and T is the out of plane thickness of the sample. Since the OOP geometry measurements exhibit a current signal at the limit of our hardware, only a lower bound of $\rho_z \geq 5\times10^{14}\ \Omega\cdot\text{cm}$ can be calculated for all three doping regimes. This value is comparable to that measured previously in half hydrogen and half hydroxide terminated silicane [$SiH_{0.5}(OH)_{0.5}$] at 250 °C [23].

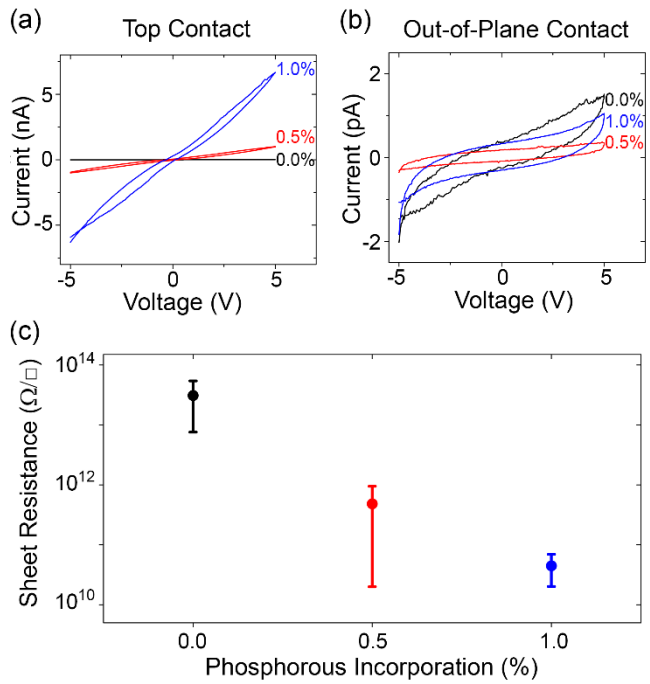

Figure 4. Doping dependence of GeH samples with 0.0% (black data), 0.5% (red data), and 1.0% (blue) incorporation of phosphorous in the $CaGe_2$ precursor. Representative I-Vs in the top-contact (a) and out-of-plane (b) geometries. Out-of-plane I-Vs show a signal below the limits of the hardware setup. (c) Sheet resistances in top-contact geometry samples for different doping regimes. Error bars represent the sample to sample variation.

On the other hand ρ_x cannot be directly extracted from the TC geometry measurements due to the non-uniformity of the current distribution which is a combination of in-plane and out-of-plane current paths. Further, the strong atmospheric dependence observed in the TC geometry implies transport in this geometry is more sensitive to the surface of the sample (and hence ρ_x) than it is to the bulk of the sample (and ρ_z). This suggests an anisotropy between ρ_x and ρ_z that is partially due to the atmospheric activation of dopants present in the samples. In order to probe this current distribution in the TC measurement and to place bounds on ρ_x (and hence the anisotropy between ρ_x and ρ_z), we developed a finite element model of transport inside of multilayered 2D materials.

3.3 Finite Element Modelling of In-Plane Resistivity

The finite element model used here is illustrated in figure 5(a). The bulk crystal is modeled by a network of in-plane and out-of-plane resistors with resistances R_x and R_z, respectively. This simple model can be modified to incorporate two materials with different internal resistance values by stacking blocks of materials on top of each other, each with their own internal resistances. We use primed variables to refer to the resistances (R_x' and R_z') in the top material block, and unprimed variables (R_x and R_z) to note the

resistances in the lower block. This network of resistors can then be solved for the equivalent sheet resistance of the complete network. The values of network resistors are tuned in order to match this equivalent sheet resistance to the measured sheet resistance. Additionally, this model yields the voltage at each node and the current across the resistors between nodes. The input model resistances R_{x} and R_{z} for both layers can be directly related to the physical resistivities of the materials of the different blocks (ρ_{x} and ρ_{z}) through the relations:

$$R_{\mathrm{x}} = \rho_{\mathrm{x}}\left(\frac{l}{t \cdot w}\right) \quad \text{and} \quad R_{\mathrm{z}} = \rho_{\mathrm{z}}\left(\frac{t}{l \cdot w}\right)$$

where $l, t,$ and w are the physical cell dimensions used to describe the model. In the case of GeH, we let $l = t = 0.6$ nm—the thickness of a physical GeH sheet—and let w be the width of the samples themselves. This network of resistors is solved analytically using Kirchhoff's circuit laws to generate a set of linear equations which are solved for the voltage at each node, the current across each resistor, and the equivalent sheet resistance of the network as a whole. The model was implemented using National Instruments (NI) LabVIEW software along with NI's multicore analysis and sparse matrix toolkit. We apply this model to the 0.5% P:GeH measurements.

To extract the in-plane resistivity of the P:GeH, the ρ_{z} value extracted from OOP measurements is held constant, while ρ_{x} is iterated until the equivalent sheet resistance of the model matches the sheet resistance measured in the TC geometry (R_{TC}). The vacuum measurements (black curves in figures 2(b) and 2(d)) are simply modeled by a single block of material. Using the sheet resistance of $R_{\mathrm{TC}} = 1.0 \times 10^{14}$ Ω/□ measured in the TC geometry and $\rho_{\mathrm{z}} = 5 \times 10^{14}\ \Omega \cdot \mathrm{cm}$, extracted from OOP geometry measurement, the in-plane resistivity is calculated to be $\rho_{\mathrm{x}} = 1.4 \times 10^{7}\ \Omega \cdot \mathrm{cm}$. This resistivity is four orders of magnitude smaller than the in-plane resistivity measured in the half hydrogen and half hydroxide terminated silicane [$SiH_{0.5}(OH)_{0.5}$] at 250 °C, and twelve orders of magnitude smaller than the extrapolated room temperature value [23].

To model the resistivities of the samples exposed to water vapor (I-V measurements shown in blue curves in figures 2b and 2d), the two block model is used. Here, the top block is made up of a number of surface layers in which the atmosphere has water activated carriers (assigned values of ρ_{x}' and ρ_{z}') while the second block is the non-activated bulk (assigned values of ρ_{x} and ρ_{z}). The value for ρ_{x} and ρ_{z} are the same values extracted from the vacuum measurements ($\rho_{\mathrm{x}} = 1.4 \times 10^{7}\ \Omega \cdot \mathrm{cm}, \rho_{\mathrm{z}} = 5 \times 10^{14}\ \Omega \cdot \mathrm{cm}$). The values of ρ_{x}' and ρ_{z}' are then varied so that the equivalent sheet resistance of the network matches the observed sheet resistance of $R_{\mathrm{TC}} = 3.8 \times 10^{10}$ Ω/□. The number of water activated layers is varied in the model as a means of accounting for the surface roughness in the measured samples.

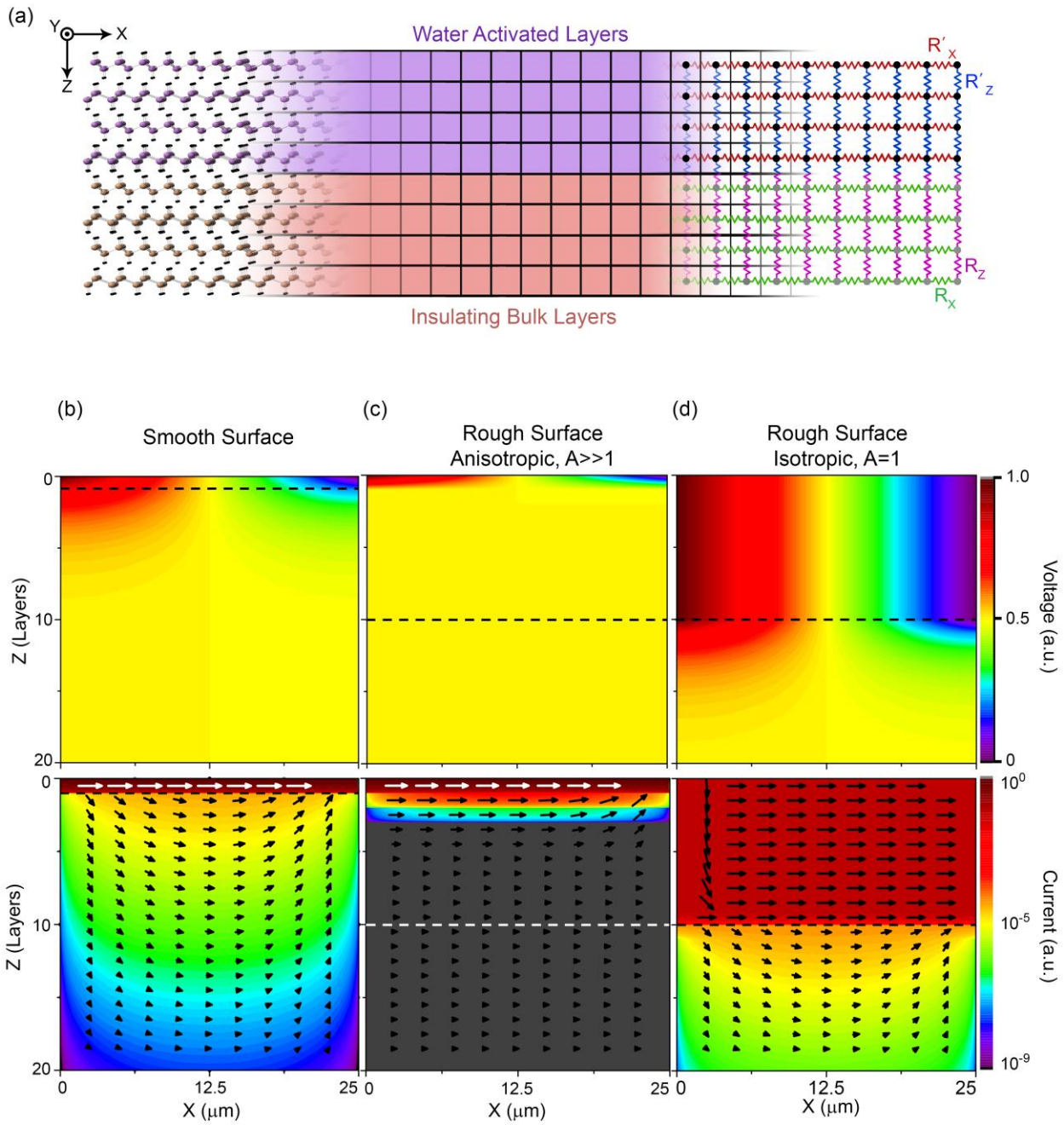

Figure 5. (a) Cartoon showing the model developed to investigate current flow in a layered, multi-material structure. Material layers are split into cells with dimensions equal to that of a single layer thickness. Material resistances (in-plane and out-of-plane) are input as the pairs R'_x, R'_z and R_x, R_z, and the network of resistors is solved for the voltage at each voltage node (V_n) and the equivalent resistance of the network. Voltage and current maps—top and bottom of (b), (c), and (d), respectively—are shown for a smooth surface (a), a rough surface with anisotropic conductivity in the water activated 0.5% P:GeH block (b), and a rough surface with isotropic conductivity in the water activated P:GeH block (c). The smooth surface is simulated using one single layer of water activated P:GeH, while rough surfaces are simulated with ten layers of water activated P:GeH. Dashed lines distinguish between the upper water activated block, and the bottom non-water activated block of the model.

Rougher samples are expected to have a higher number of layers exposed to the atmosphere while an atomically smooth sample would only have the single topmost layer exposed to the atmosphere. For this reason, a rougher sample is modeled assuming the top ten layers of GeH are water activated, while a smooth sample assumes only the top layer is water activated.

For the case of an atomically smooth sample we assume that only a single layer of material experiences water activation of dopants, thus there is no ρ_z' value and only ρ_x' is varied until the effective sheet resistance matches the observed sheet resistance. This occurs at $\rho_x' = 2.3 \times 10^3\ \Omega \cdot \text{cm}$. The resultant current and voltage maps for this case are shown in figure 5(b). Modeling indicates that in this case, >99% of the current travels solely in this topmost layer. The modeled ρ_x' value is nearly four orders of magnitude smaller than the value derived in the unactivated case ($\rho_x = 1.4 \times 10^7\ \Omega \cdot \text{cm}$), and eleven orders smaller than the out of plane resistivity ($\rho_z = 5\times10^{14}\ \Omega\cdot \text{cm}$).

A more realistic view of the P:GeH samples is that the surface is not atomically flat. In this scenario, several layers are exposed to the atmosphere and experience dopant activation. To model this, the top ten layers of the sample are assumed to be water activated. This corresponds to a roughness of 6 nm. While water is unlikely to diffuse through the bulk of the GeH samples and change the OOP resistance measurements, the measured currents in the OOP geometry are below the minimum instrument resolution, making it impossible to verify this hypothesis. Consequently, we chose to model two extreme cases for the for the P:GeH anisotropy, $A = \rho_z'/\rho_x'$. The first assumes no change in ρ_z' compared to the vacuum measurements ($A \gg 1$) so that the water has no effect on the OOP resistivity. The second case assumes a large reduction in ρ_z' due to the water activation ($A = 1$).

For the strong anisotropy ($A \gg 1$) case, $\rho_z' = 5 \times 10^{14}\ \Omega \cdot \text{cm}$, the value calculated from the OOP measurements. Here, $\rho_x' = 2.3 \times 10^3\ \Omega \cdot \text{cm}$, the same as the previously modeled smooth sample. The result for this scenario is shown in figure 5(c). Again >99% of the current flows through the topmost layer. The final case (figure 5(d)) again assumes ten layers of water activated GeH, but this time the water activation is taken to increase the interlayer conduction yielding isotropic resistivity values, $A = 1$. In this case values of $\rho_x' = \rho_z' = 2.3 \times 10^4\ \Omega \cdot \text{cm}$ are extracted from the model. Here, >99% of the current travels inside of the water activated region and is equally distributed throughout these surface layers.

A summary of the modeling results is shown in table 1. In all three cases, we find that the value of the in-plane resistivity is bounded $2.3 \times 10^3 < \rho_x' < 2.3 \times 10^4\ \Omega \cdot \text{cm}$, which is 10 - 11 orders of magnitude smaller than the calculated out-of-plane resistivity value of $\rho_z = 5 \times 10^{14}\ \Omega \cdot \text{cm}$. Additionally, >99% of the current is confined to only the water activated layers of the sample in all of the modeled cases.

Table 1. Summary of modeling results for the cases involving water activated dopants.

Number of Activated Layers	ρ_z' ($\Omega \cdot$ cm)	ρ_x' ($\Omega \cdot$ cm)	A = ρ_z'/ρ_x'
1	5×10^{14}	2.3×10^{3}	2.2×10^{11}
10	5×10^{14}	2.3×10^{3}	2.2×10^{11}
10	2.3×10^{4}	2.3×10^{4}	1

4. Conclusion

We have grown both doped and undoped GeH crystals and evaluated their transport properties for the first time. By incorporating phosphorous into the synthesis of the $CaGe_2$ precursor, it is possible to electronically dope GeH, leading to a reduction in the sample resistance by up to three orders of magnitude. Electrical transport measurements conducted on bulk crystalline GeH samples using two different contact geometries show a large resistance anisotropy between the in-plane and out-of-plane directions. The resistivity of the crystals exhibit a strong atmospheric dependence with the resistivity decreasing by up to three orders of magnitude when samples are exposed to air. This atmospheric dependence of the resistance, along with the photocurrent measurements suggest that the presence of water vapor in the air is activating dopants on the surface of the P:GeH crystals. To better understand the current distribution inside these layered materials, we developed a finite element model which indicates that nearly all of the current travels in the topmost water activated layers. These experimental and modeling results suggest the possibility of the ability to measure exotic single layer properties in the top layer of a multilayered group IV graphane crystal by making electronic contact to the top surface.

5. Acknowledgments

Primary support for this work, especially electrical characterization and modeling comes from the Center for Emergent Materials at The Ohio State University, an NSF MRSEC center (Grant DMR-1420451). Partial support for materials synthesis comes from the Army Research Office (Grant W911-NF-12-1-0481).

[1] Novoselov K S, Geim A K, Morozov S V, Jiang D, Katsnelson M I, Grigorieva I V, Dubonos S V and Firsov A A 2005 Two-dimensional gas of massless Dirac fermions in graphene *Nature* **438** 197-200
[2] Radisavljevic B, Radenovic A, Brivio J, Giacometti V and Kis A 2011 Single-layer MoS2 transistors *Nat. Nanotechnol.* **6** 147-50
[3] Frindt R F 1972 Superconductivity in Ultrathin NbSe2 Layers *Phys. Rev. Lett.* **28** 299-301
[4] Frindt R F 1966 Single Crystals of MoS2 Several Molecular Layers Thick *J. Appl. Phys.* **37** 1928-9
[5] Allen M J, Tung V C and Kaner R B 2009 Honeycomb carbon: a review of graphene *Chem. Rev.* **110** 132-45
[6] Gong Y, *et al.* 2014 Vertical and in-plane heterostructures from WS2/MoS2 monolayers *Nat. Mat.* **13** 1135-42
[7] Geim A K and Novoselov K S 2007 The rise of graphene *Nat. Mat.* **6** 183-91
[8] Eda G and Maier S A 2013 Two-Dimensional Crystals: Managing Light for Optoelectronics *ACS Nano* **7** 5660-5
[9] Zhang Y, Tan Y-W, Stormer H L and Kim P 2005 Experimental observation of the quantum Hall effect and Berry's phase in graphene *Nature* **438** 201-4
[10] Mak K F, Lee C, Hone J, Shan J and Heinz T F 2010 Atomically thin MoS2: a new direct-gap semiconductor *Phys. Rev. Lett.* **105** 136805
[11] Splendiani A, Sun L, Zhang Y, Li T, Kim J, Chim C-Y, Galli G and Wang F 2010 Emerging photoluminescence in monolayer MoS2 *Nano Lett.* **10** 1271-5
[12] Chhowalla M, Shin H S, Eda G, Li L-J, Loh K P and Zhang H 2013 The chemistry of two-dimensional layered transition metal dichalcogenide nanosheets *Nat. Chem.* **5** 263-75
[13] Voiry D, Goswami A, Kappera R, e Silva C d C C, Kaplan D, Fujita T, Chen M, Asefa T and Chhowalla M 2015 Covalent functionalization of monolayered transition metal dichalcogenides by phase engineering *Nat. Chem.* **7** 45-9
[14] Jiang S, Butler S, Bianco E, Restrepo O D, Windl W and Goldberger J E 2014 Improving the stability and optical properties of germanane via one-step covalent methyl-termination *Nat. Commun.* **5**
[15] Arguilla M Q, Jiang S, Chitara B and Goldberger J E 2014 Synthesis and Stability of Two-dimensional Ge/Sn Graphane Alloys *Chem. Mater.* **26** 6941-6
[16] Bianco E, Butler S, Jiang S, Restrepo O D, Windl W and Goldberger J E 2013 Stability and exfoliation of germanane: a germanium graphane analogue *ACS Nano* **7** 4414-21
[17] Vogg G, Brandt M and Stutzmann M 2000 Polygermyne—a prototype system for layered germanium polymers *Adv. Mater.* **12** 1278-81
[18] Xu Y, Yan B, Zhang H-J, Wang J, Xu G, Tang P, Duan W and Zhang S-C 2013 Large-gap quantum spin Hall insulators in tin films *Phys. Rev. Lett.* **111** 136804
[19] Butler S Z, *et al.* 2013 Progress, Challenges, and Opportunities in Two-Dimensional Materials Beyond Graphene *ACS Nano* **7** 2898-926
[20] Edman L, Sundqvist B, McRae E and Litvin-Staszewska E 1998 Electrical resistivity of single-crystal graphite under pressure: An anisotropic three-dimensional semimetal *Physical Review B* **57** 6227-30
[21] Pinchuk I V, Odenthal P M, Ahmed A S, Amamou W, Goldberger J E and Kawakami R K 2014 Epitaxial co-deposition growth of CaGe2 films by molecular beam epitaxy for large area germanane *J. Mater. Res.* **29** 410-6
[22] Tao L, Cinquanta E, Chiappe D, Grazianetti C, Fanciulli M, Dubey M, Molle A and Akinwande D 2015 Silicene field-effect transistors operating at room temperature *Nat. Nanotechnol.* **10** 227-31
[23] Brandt M, Puchert T and Stutzmann M 1997 Electronic transport in crystalline siloxene *Solid State Commun.* **102** 365-8
[24] Sarma S D, Adam S, Hwang E H and Rossi E 2011 Electronic transport in two-dimensional graphene *Rev. Mod. Phys.* **83** 407

[25] Baugher B W H, Churchill H O H, Yang Y and Jarillo-Herrero P 2013 Intrinsic electronic transport properties of high-quality monolayer and bilayer MoS2 *Nano Lett.* **13** 4212-6

[26] Dresselhaus M S and Dresselhaus G 1981 Intercalation compounds of graphite *Adv. Phys.* **30** 139-326